

On the Possible Properties of Small and Cold Extrasolar Planets: Is OGLE-2005-BLG-390Lb Entirely Frozen?

David Ehrenreich, Alain Lecavelier des Etangs, and Jean-Philippe Beaulieu

*Institut d'astrophysique de Paris
CNRS (UMR 7095) ; Université Pierre & Marie Curie
98 bis, boulevard Arago 75014 Paris, France*

ehrenreich@iap.fr

and

Olivier Grasset

*Laboratoire de planétologie et de géodynamique
CNRS (UMR 6112) ; Université de Nantes
2, rue de la Houssinière 44322 Nantes, France*

ABSTRACT

Extrasolar planets as light as a few Earths are now being detected. Such planets are likely not gas or ice giants. Here, we present a study on the possible properties of the small and cold extrasolar planets, applied to the case of the recently discovered planet OGLE-2005-BLG-390Lb (Beaulieu et al. 2006). This planet ($5.5^{+5.5}_{-2.7}$ Earth masses) orbits $2.6^{+1.5}_{-0.6}$ -astronomical units away from an old M-type star of the Galactic Bulge. The planet should be entirely frozen given the low surface temperature (35 to 47 K). However, depending on the rock-to-ice mass ratio in the planet, the radiogenic heating could be sufficient to make the existence of liquid water within an icy crust possible. This possibility is estimated as a function of the planetary mass and the illumination received from the parent star, both being strongly related by the observational constraints. The results are presented for water-poor and water-rich planets. We find that no oceans can be present in any cases at 9–10 Gyr, a typical age for a star of the Bulge. However, we find that, in the past when the planet was $\lesssim 5$ billion years old, liquid water was likely present below an icy surface. Nevertheless, the planet is now likely to be entirely frozen.

Subject headings: planetary systems — stars: individual (OGLE-2005-BLG-390L)

1. INTRODUCTION

Some 190 extrasolar planets have been detected since 1992.¹ Most of these discoveries have been performed using radial velocimetry. Recent progresses and new instruments have permitted the lowering of the mass detection threshold to tens of Earth masses (M_{\oplus}). For instance, a $14\text{-}M_{\oplus}$ ($\times \sin i$, where i is the inclination of the planet orbital plane) planet around the star μ Arae (Santos et al. 2004), a $7.5\text{-}M_{\oplus}$ planet around GJ 876 (Rivera et al. 2005), and a $10\text{-}M_{\oplus}$ planet around HD 69 830 (Lovis et al. 2006) have been reported. All these objects lie at the mass boundary between telluric and ice giant planets, as it is inferred from analogy with the Solar System ice giants, Uranus and Neptune (14.5 and $17.2 M_{\oplus}$, respectively). Besides, all low-mass planets discovered with radial velocimetry are orbiting very close to their parent stars, $\lesssim 0.1$ astronomical units (AU), so they are enduring extreme radiative heating (Lecavelier des Etangs 2006), an unknown situation in the Solar System. Indeed, the radial-velocity technique is biased towards short-orbital-period planets.

On the contrary, the microlensing technique is sensible to planets with larger semi-major axis, hence it allows to detect a different kind of planets. Using this technique, Beaulieu et al. (2006) have detected a $5.5_{-2.7}^{+5.5}\text{-}M_{\oplus}$ planet orbiting at $2.6_{-0.6}^{+1.5}$ AU from a $0.22_{-0.11}^{+0.21}$ -solar-mass (M_{\odot}) star. It is potentially the lightest exoplanet detected so far. This star and its planet are the lens of the gravitational microlensing event OGLE-2005-BLG-390 (see Table 1) and the star, according to its mass range, is a M star, with a luminosity reaching only ~ 0.01 solar luminosity (L_{\odot}). Hence, the amount of energy per surface unit this planet receives from its star is comparable to that of Pluto in the Solar System ($\sim 0.1 \text{ W m}^{-2}$). The planet detected by Beaulieu et al. (2006), poetically designated as OGLE-2005-BLG-390Lb, is thus a cold sub-Uranus object.

In the light of the orbital elements and masses presented in Beaulieu et al. (2006), the planet can be a cold and massive analog of the Earth, or alternatively be similar to a frozen ocean-planet having retained a lot of water (Léger et al. 2004). In both cases, the question arises if the planet is entirely frozen or if liquid water can exist close to the surface. To answer that question, we focus on the phase study of water (H_2O) in the first ~ 100 km under the planetary surface, using observational constrains and similarities with icy satellites of the Solar System. A full model of the entire planet is certainly beyond the scope of the present work (see Sotin et al. 2006 for a detailed study of the internal structure of these kinds of extrasolar planets).

¹From J. Schneider’s *Extrasolar planets encyclopaedia* at <http://vo.obspm.fr/exoplanetes/encyclo/encycl.html>.

2. ASSUMPTIONS AND BASIC PROPERTIES OF OGLE-2005-BLG-390Lb

All the parameters of the lens system deduced from the detection are related to the mass of the lens star M_\star . The mass of the planet M_P is simply given by the relation

$$M_P = q \times M_\star, \quad (1)$$

where q is the planet-to-star mass ratio measured by Beaulieu et al. (2006) and given in Table 1. We took advantage of these correlations (eqs. [1, 2, and 3]) to estimate the basic properties of the system as a function of the stellar and planetary masses, such as the semi-major axis of the planet and the stellar luminosity (§ 2.1). Then, we calculated the energy the planet is receiving from its star and its equilibrium temperature, again as a function of the planetary mass (§ 2.2). Given the surface temperature and the atmospheric scale height, we then discuss on the possible nature of an atmosphere (§ 2.3).

2.1. Constraints from the Microlensing Event

The microlensing event OGLE-2005-BLG-390 is described by Beaulieu et al. (2006), and the relevant parameters for this study are presented in Table 1. All the parameters are in fact represented by a Bayesian distribution of probability. We have explored the phase space allowed by the results presented in the above-cited paper.

Beaulieu et al.’s analysis (based on Dominik 2006) yields 95% probability that the lens star be a main sequence star, 4% that it be a white dwarf, and less than 1% that it be a neutron star or a black hole. They find a 75% probability that the star be part of the Galactic Bulge. When adopting a source star distance of 8.5 kpc, the lens star is estimated to be 6.6 ± 1.0 -kpc away, toward the Galactic Center. Zoccali et al. (2003) have shown that the Bulge is about 10-billion-years (Gyr) old with no evidence for younger stellar populations. They also proved that the Bulge metallicity is peaked near the solar value, with a sharp cutoff just above this value and a tail towards lower metallicity. As part of the Bulge population, we therefore consider that the lens system (star and planet) is likely to be ~ 10 -Gyr old, with a solar metallicity.

The mass of the stellar lens derived from Beaulieu et al. is $M_\star \approx 0.22 M_\odot$, within a range $[0.11, 0.43] M_\odot$,² i.e., most probably the mass of a M-type star. In that range and using eq. (1), the planetary mass is found within $[3, 11] M_\oplus$; the planet has more than 95% probability to be lighter than Uranus.

²The quantity accurately measured by Beaulieu et al. (2006) is the planet-to-star mass ratio q .

The separation of the lens d is expressed in Einstein’s radii, R_E . From the equation defining R_E as a function of M_\star (see Table 1 in Beaulieu et al. 2006), the semi-major axis a of the planet can be expressed as

$$\frac{a}{1 \text{ AU}} = 0.53 + 9.76 \frac{M_\star}{M_\odot} - 6.30 \left(\frac{M_\star}{M_\odot} \right)^2 + 2.59 \left(\frac{M_\star}{M_\odot} \right)^3. \quad (2)$$

Given the stellar-mass range explored, a is within [1.5,3.8] AU.

To estimate the surface temperature of OGLE-2005-BLG-390Lb (see § 2.2) we need first estimate the stellar luminosity L_\star . This is done using a mass-luminosity relation derived from Baraffe et al. (1998) for a solar metallicity, (see also Beaulieu et al. 2006b, in preparation)

$$\begin{aligned} \log_{10} \frac{L_\star}{L_\odot} &= -0.04 + 6.03 \log_{10} \frac{M_\star}{M_\odot} + 4.16 \left(\log_{10} \frac{M_\star}{M_\odot} \right)^2 \\ &\quad - 2.19 \left(\log_{10} \frac{M_\star}{M_\odot} \right)^3 - 3.37 \left(\log_{10} \frac{M_\star}{M_\odot} \right)^4. \end{aligned} \quad (3)$$

Considering again the same stellar-mass range than above, the luminosity of the planet host star should be within [0.001,0.02] L_\odot . This result would be barely changed by assuming a different metallicity than solar; for instance, a 0.5-dex decrease in metallicity would increase the luminosity by $\sim 20\%$ (still according to Baraffe et al. 1998), then triggering only a ~ 1 -K increase in the surface temperature of the planet (see below).

2.2. Energy Received from the Star

From the semi-major axis of the planet and the stellar luminosity, it is straightforward to calculate the amount of energy received by the planet and thus its equilibrium surface temperature, which also depends on the surface albedo. The power received per surface unit is $q_\star = L_\star / (16\pi a^2)$, i.e., within [0.2,0.8] W m^{-2} . This is roughly the same amount of energy received by Pluto or Neptune from the Sun. Analogously to the outer planets of the Solar System, which formed and remained beyond the snowline, OGLE-2005-BLG-390Lb can contain an important fraction of volatile material (ices) and thus resemble a massive Ganymede with frozen surface.

We then assume an albedo A of 50% for an ice-covered surface and calculate the surface temperature of the planet, taken to be the equilibrium temperature,

$$T_{\text{surf}} \approx T_{\text{eq}} = \sqrt[4]{\frac{L_\star (M_\star) (1 - A)}{16\pi a^2 \sigma}}, \quad (4)$$

where σ is the Stefan-Boltzmann constant and $L_\star(M_\star)$ is the stellar luminosity as a function of the stellar mass, as given by eq. (3). As M_\star is related to M_P through eq. (1), the stellar luminosity is also a function of M_P . Figure 1 represents the surface temperature as a function of the planetary mass. Considering the parameter range given above, T_{surf} is within [35,47] K.

2.3. Atmosphere

Given the surface temperature range, the vapor pressure of most volatile species of interest (H_2O , methane CH_4 , ammonia NH_3 , carbon dioxide CO_2) is very weak, below 0.01 Pa. Only carbon monoxide (CO) and molecular nitrogen (N_2) have relatively high vapor pressures at these temperatures ($p_{\text{CO}_2} \approx 100$ Pa at 47 K, $p_{\text{N}_2} \approx 0.1$ Pa at 35 K). Moreover, N_2 starts sublimating around 47 K, where $p_{\text{N}_2} \approx 100$ Pa.³ Thus, these two species are the most likely to be present in the planetary atmosphere.

For a planetary mass within [3,11] M_\oplus , and given the radii we estimate in § 3.1, the surface gravity of OGLE-2005-BLG-390Lb lies within [10,30] m s^{-2} . We consequently estimate the atmospheric scale height for N_2 or CO to be within [0.5,1] km. Considering the small scale height and vapor pressure for N_2 , we hypothesize the presence of a tenuous atmosphere of N_2 with a surface pressure $p_0 = p_{\text{N}_2} \sim 1$ hPa. Note that the atmospheric pressure measured at the surface of Pluto (0.5 Pa according to Sicardy et al. 2003) is lower than the vapor pressure of N_2 at Pluto’s surface temperature (~ 40 K), therefore, the nitrogen vapor pressure of 1 hPa can be considered as an upper limit to the actual atmospheric pressure in our case. Anyway, it is a fairly weak value, insignificant for the calculation of the ice shell structure (see § 4). We further take an atmospheric pressure at the surface $p_0 \approx 0$.

The main properties of OGLE-2005-BLG-390Lb deduced from the measurements of Beaulieu et al. (2006) suggest an extremely cold surface. If liquid water is to exist somewhere in this planet, it is very likely below an icy crust, as in the icy satellites of the Solar System.

3. STRUCTURE OF THE PLANET

We saw in the previous section that liquid water cannot exist on the surface of OGLE-2005-BLG-390Lb because of the low temperature and pressure. Instead, the surface of the

³Vapor pressure data can be found for various species on Air Liquide’s Gas Encyclopaedia website at <http://encyclopedia.airliquide.com> while temperatures for different vapor pressures may be found on AVS Technical Resources’ website at <http://www.aip.org/avsguide/refguide/vapor.html>.

planet should be frozen ice. The question is then: can liquid water exist below the ice layer? A description of the physical states of water in the ice shell can be obtained using a phase diagram and knowing the evolution of the pressure and temperature within the ice shell. The pressure at a depth z in the ice shell is

$$p(z) = \int_0^z \rho(x)g(x)dx; \quad (5)$$

it depends on the gravity of the planet, hence on its radius.

3.1. Internal Structure and Radius of OGLE-2005-BLG-390Lb

Models of possible internal structures for Earth-mass extrasolar planets have already been developed. The radius of OGLE-2005-BLG-390Lb is found using such a model (Sotin et al. 2006), which a basic version has been used by Léger et al. (2004) for the modeling of ‘ocean-planets’. Its physical approach is analogous to that of Valencia et al. (2006). The main difference is that the bulk composition of the planet is fixed by the composition of the star. The input parameters are the stellar iron-to-silicium $[\text{Fe}/\text{Si}]$ and magnesium-to-silicium $[\text{Mg}/\text{Si}]$ ratios, the magnesium content of the silicate mantle $\text{Mg}_{\#} = [\text{Mg}/(\text{Mg} + \text{Fe})]$, the amount of H_2O , and the total mass of the planet (Sotin et al. 2006).

Solar $[\text{Fe}/\text{Si}]$ and $[\text{Mg}/\text{Si}]$ are assumed together with a terrestrial $\text{Mg}_{\#} = 0.9$. It can be noted that varying these numbers from the solar and terrestrial values changes the size of the metallic core (composed by Fe and iron sulphide FeS) and the amount of Fe in the silicate mantle, but causes small differences on the computed planetary radii (3/1000 in average). On the contrary, the amount of H_2O strongly influences the radius for a given planetary mass. We consider different enrichments of the planet in H_2O , namely 0.025, 25, and 50% of the planetary mass.⁴

Mass-radius relationships are then derived using appropriate equations of state for the different layers. The Mie-Grüneisen-Debye formulation has been chosen for describing the iron core (Uchida et al. 2001), the lower silicate mantle (Hemley et al. 1992) and the icy mantle (Fei et al. 1993). The 3rd-order Birch-Mürnaghan equation of state is used for the upper silicate mantle (Vacher et al. 1998) and for the liquid layer (Lide 2005).

The 0.025%wt- H_2O case corresponds to a rocky planet with a H_2O content similar to the Earth one. The model yields a structure consisting of a metallic core accounting for

⁴In the following, fractions of water will be given as fractions of the planetary mass and noted as weight-percentages (%wt).

32%wt and a rocky mantle (silicates) accounting for $f_{\text{sil}} = 68\%$ wt, where f_{sil} represents the mass fraction of silicates in the planet. The resulting radius is within $[1.3, 2.0] R_{\oplus}$ depending on the planetary mass.

For both other cases, 25 and 50%wt- H_2O , the silicate-mantle-to-iron-core mass ratio remains similar to the 0.025%wt case, i.e., about 2/1. Over the whole planet, the silicates must account for $f_{\text{sil}} = 0.68 \times (1 - 0.25) = 51\%$ wt and $f_{\text{sil}} = 0.68 \times (1 - 0.5) = 34\%$ wt in the 25 and 50%wt cases, respectively. Planetary radii are found within $[1.4, 2.3] R_{\oplus}$ and $[1.6, 2.5] R_{\oplus}$, respectively, depending on the planetary mass. These results are summarized in Fig. 2.

3.2. Phases of Ice in the Icy Mantle

Due to the low surface temperature, the volatile material present in OGLE-2005-BLG-390Lb must be condensed as an ice shell. Since the planet is massive enough to be completely differentiated, the ice shell must be overtopping a denser rocky core, in a situation similar to that of the icy moons of giant planets in the Solar System.

3.2.1. The Water-Poor Case (0.025%wt)

If the planet contains the same proportion of water than the Earth, that is, very few: $2.5 \times 10^{-4} M_P$, the maximum pressure at the bottom of the ice shell is $p_{\text{ice}} \approx M_{\text{ice}} g / (4\pi R_P^2)$, where g is within $[15, 29] \text{ m s}^{-2}$ for a planetary mass in $[3, 11] M_{\oplus}$. Then, $p_{\text{ice}} \approx 2.5 \times 10^{-4} g^2 / (4\pi G)$, i.e., within $[0.07, 0.25] \text{ GPa}$. Therefore, from the phase diagram of water represented in Fig. 3,⁵ the ice shell is only composed of ice I or possibly a liquid layer surrounded by a thin layer of ice I. Using eq. (5), the depth of the interface ice I/silicates or liquid/silicates is found within $[5, 9] \text{ km}$ (see Fig. 4). Consequently, the icy mantle that covers the silicates is rather small compared to the planetary radius; it consists of a thin ($\lesssim 10 \text{ km}$) low-pressure ice-I layer.

⁵A full phase diagram of H_2O is available on the website *Water structure and behavior* by M. Chaplin, at <http://www.lsbu.ac.uk/water/phase.html>.

3.2.2. The Water-Rich Case (25 and 50%wt)

If a non-negligible fraction of the planetary mass is accounted for by water, then the ice shell must be largely composed of high-pressure ice due to the strong gravity (from 10 to 22 ms^{-2} depending on the planetary mass and the mass percentage of H_2O). The most stable phase at low temperature (10 to 200 K) and moderate pressure (0.2 to 0.6 GPa) is ice II; at higher pressures (deeper in the planet), we successively meet ice VI, VII, and X (those last two phases lie beyond the pressure scale in Fig. 3, at pressure greater than 2 GPa). Indeed, we find p_{ice} within [40,210] GPa, well in the domain of high-pressure ices. In such a case, the icy mantle must be split into an upper thin low-pressure ice-I/II layer and a thick high-pressure layer composed by ices V, VI, VII, and X. Actually, there is an important endothermic frontier at the phase transitions ice II/V and II/VI, which is located around $p_{\text{II}} = 0.62$ GPa (Bercovici et al. 1986). With eq. (5), we estimated the ice-I/II layer is never thicker than about 60 km (Fig. 5). Hence, in this case we distinguish between a thin ($\lesssim 60$ km) low-pressure ice (I/II) and a thick ($\sim 1\,000$ km) high-pressure ice (VI/VII) mantle.

In any cases, an entirely-solid ice shell is overtopped by a layer of low-pressure ice I. If there is not much ice in the planet (§ 3.2.1), the whole ice shell is ice I. On the contrary, if the amount of ice in the planet is large (§ 3.2.2), high-pressure phases of H_2O must be found below the ice-I lid. Because of the negative slope of the melting curve of ice I as a function of pressure, a liquid layer could only exist between ice I and silicates or between ice I and high-pressure ices. Considering the low surface temperature on OGLE-2005-BLG-390Lb ($T_{\text{surf}} \ll 250$ K) and an adiabatic ocean⁶ below ice I, the bottom of the ocean must be at pressure $\lesssim 0.6$ GPa. Therefore, due to the high gravity on OGLE-2005-BLG-390Lb, the thickness of such an ocean must be smaller than about 50 km.

3.3. Heat Flow from the Silicate Mantle

The internal heat flow determines the temperature profile within the planet, and particularly within the ice layer. Knowing that the most probable age of OGLE-2005-BLG-390Lb is 10 Gyr, the main source of internal heat at present time is the decay of long-lived radioactive isotopes of uranium (^{238}U and ^{235}U), thorium (^{232}Th), and potassium (^{40}K). Another

⁶In the following, the term ‘ocean’ is used even when referring to a layer of liquid water below an ice-I shell. In fact, what we describe here is a global liquid layer that spans within the whole planet, hence it shares similarity with the etymological origin for ‘ocean’, i.e., the river Okeanos (*ὠκεανός ποταμός*) that encircles the world in the Greek mythology.

non-negligible contribution to the heat flow is the secular cooling of the residual heat produced during the planet formation (20% for the Earth according to Turcotte & Schubert 2001). In the following, we assume that the present heat flow is equal to the radiogenic heat flow.

We take the mass fractions of the radioactive isotopes in the planet when it was 4.56-Gyr old similar to those of the Earth at the present time. Then, we calculate the heat produced by the decay of the long-lived isotopes, or radiogenic heat q_R . The mass fraction $X(t)$ of a given species at a given time t , in Gyr, is (Turcotte & Schubert 2001)

$$X(t) = X_{\oplus} \exp \left[(4.56 - t) \frac{\ln 2}{\tau_{1/2}} \right], \quad (6)$$

where X_{\oplus} is the terrestrial mass fraction of the species nowadays and $\tau_{1/2}$ is its half-life. Both are given in Table 2. The internal heat production due to the radiogenic decay, per unit of mass and at a time t , is simply $h_{\text{rad}} = \sum_i h_i X_i(t)$, where h_i is the heat produced by the species i per unit of mass given in Table 2. Finally, the heating per unit of mass of silicate mantle is $6.2 \times 10^{-12} \text{ W kg}^{-1}$ at the age of 4.56 Gyr, but it is only $3.2 \times 10^{-12} \text{ W kg}^{-1}$ at 10 Gyr, likely the age of OGLE-2005-BLG-390Lb.

More generally, the heat production is proportional to the abundances of the radioactive isotopes within the silicates. Shall the planet contain radioactive material more abundantly than Earth, it would indeed produce more heating. The effects of a varying heat production are dealt with in § 5.3.

In the following, we use the radiogenic heat produced per unit of mass of the planet, $h'_{\text{rad}} = h_{\text{rad}} \times f_{\text{sil}}$, where f_{sil} is the mass fraction of silicates in the planet. In fact, the radioactive isotopes are only contained in the silicate mantle of the planet, not in the metallic core nor in the ice shell. In § 3.1, we saw that f_{sil} is estimated to be 68, 51, or 34%wt, for water mass fraction of 0.025, 25, or 50%wt, respectively. At the age of 10 Gyr, this gives h'_{rad} of 2.2×10^{-12} , 1.6×10^{-12} , and $1.1 \times 10^{-12} \text{ W kg}^{-1}$, respectively.

At a depth z within the ice shell and at a time t , the heat flow generated by the radioactive isotopes is

$$q_{\text{rad}}(z, t) = \frac{h'_{\text{rad}}(t) \times M_P}{4\pi(R_P - z)^2}. \quad (7)$$

At the surface ($z = 0$), for $t = 10$ Gyr, and for M_P within [3,11] M_{\oplus} , we find q_{rad} within [40,70], [24,44], and [13,24] mW m^{-2} , in the 0.025, 25, and 50%wt cases, respectively.

4. CAN LIQUID WATER EXISTS WITHIN THE ICE SHELL?

Although liquid water cannot exist on the surface of the exoplanet OGLE-2005-BLG-390Lb (§ 2.2), a liquid layer can exist *below the low-pressure ice-I shell*. This ice shell is heated from below by the decay of radioactive elements. An adiabatic ocean can be present if the temperature profile crosses the melting curve of ice I. There are two cases to be considered:

(i) If the planet is water-poor (0.025%wt), the heat produced by silicates can be transferred either by conduction or convection across the low-pressure ice-I mantle. Examples of conductive profiles are sketched in Fig. 4.

(ii) If the planet is water-rich (25 or 50%wt), the ice mantle consists of two parts: a low-pressure ice-I/II shell and a high-pressure ice-VI/VII shell (§ 3.2.2 and Fig. 5). The high-pressure mantle allows the heat to be transferred very efficiently by convection from the silicates up to the base of the low-pressure ice-I/II mantle, at the interface II/VI (see Fig. 3). The heat is then transferred across the low-pressure ice-I/II mantle by conduction or convection, as in case (i).

The absence or presence of liquid water can be constrained by considering the extreme cases when the heat is transferred only by conduction (§ 4.1) or when the convection is set up (§ 4.2).

4.1. Conduction in the Ice

In the top layer of ice, the heat is transferred by thermal conduction to the surface of the planet. The expected temperature profiles are similar to those sketched in Figs. 4 and 5 across the low-pressure ice-I and ice-I/II layers, respectively.

The equilibrium between heat flux and heat production rate is assumed, i.e., the heat flux at the surface equals the flux heating from below (which corresponds to the internal heating by silicates, see § 3.3). The boundary conditions are: (i) at the surface, the temperature is $T_{\text{surf}} = T_{\text{surf}}(M_P)$ obtained from eqs. (1, 2, 3, and 4), and (ii) at the base of the low-pressure ice layer, the heat produced h'_{rad} is a constant related to the heat flux q through eq. (7).

The conservation of energy when there is no additional heat source within the ice layer is

$$\frac{\partial q(r)}{\partial r} + \frac{2}{r}q(r) = 0, \quad (8)$$

where $q(r)$ is the flux at a radial distance r from the planet center and is given by the Fourier

law in the purely diffusive case,

$$q(r) = -k(T) \frac{\partial T}{\partial r}, \quad (9)$$

where the thermal conductivity k obeys the empirical law

$$k(T) = k_0/T, \quad (10)$$

with $k_0 = 567 \text{ W m}^{-1}$ (Klinger 1980).

Combining eqs. (7, 8, 9, and 10), the temperature profile is

$$T(r) = T_{\text{surf}} \exp \left[\frac{h'_{\text{rad}} M_P}{4\pi k_0} \left(\frac{1}{r} - \frac{1}{R_P} \right) \right]. \quad (11)$$

The resulting profiles are plotted in Fig. 6 for the 0.025, 25, and 50%wt cases.

Let δ be the diffusive coefficient,

$$\delta(r) \equiv \frac{T(r)}{T_{\text{surf}}}. \quad (12)$$

Near the surface, we have $g \approx GM_P/R_P^2$ and then $z \approx p/\rho g$. Therefore, replacing r by $R_P - z$ in eq. (11), we get

$$\delta = \delta(p, h'_{\text{rad}}) \approx \exp \left(\frac{h'_{\text{rad}} p}{4\pi G k_0 \rho} \right). \quad (13)$$

The coefficient δ does not depend upon the planetary mass, but only on the pressure p and the heat flow h'_{rad} . Knowing the surface temperature, we can plot the temperature profile over the phase diagram, in Fig. 6.

At the pressure of $p_{\text{I}} = 0.21 \text{ GPa}$ – the pressure at the triple point I/III/liquid, see Fig. 3 – the coefficient δ is 2.8, 2.2, and 1.7 in the 0.025, 25, and 50%wt cases, respectively. Resulting temperature ranges are [100,135] K, [75,105] K, and [60,80] K for the planetary mass within [3,11] M_{\oplus} .

In the 25 and 50%wt cases, the ice pressure can reach the pressure of the next phase transition, $p_{\text{II}} = 0.61 \text{ GPa}$. Then, δ follows the law

$$\delta(p, h'_{\text{rad}}) \approx \exp \left[\frac{h'_{\text{rad}}}{4\pi G k_0} \left(\frac{p_{\text{I}}}{\rho_{\text{I}}} + (p - p_{\text{I}}) / \rho_{\text{II}} \right) \right], \quad (14)$$

where $\rho_{\text{I}} = 917 \text{ kg m}^{-3}$ and $\rho_{\text{II}} = 1600 \text{ kg m}^{-3}$ are the density of ice I and ice II. We find δ is 7.3 and 3.7 for the 25 and 50%wt cases, respectively. As the heat is transferred by thermal conduction, by using the approximation $T(p_{\text{II}}) \approx \delta(p_{\text{II}}) T_{\text{surf}}$, we get temperatures within [250,340] K and [130,175] K in the 25 and 50%wt cases, respectively.

4.2. Convection in the Ice

Unlike conduction, convection is an efficient heat transfer mechanism. If convection is possible in the solid ice shell of OGLE-2005-BLG-390Lb, then the temperature profile can be described as, starting from the surface: a thin conductive lid of ice, an upper thermal boundary layer (TBL), a well-mixed adiabatic ice layer where the temperature T_{conv} is nearly constant, and a lower thermal boundary layer (Hussmann et al. 2002; Spohn & Schubert 2003; Sotin & Tobie 2004).

According to Spohn & Schubert (2003), the thermal flux through the convective ice layer is

$$q_{\text{conv}} = b \left(\frac{\alpha g}{\kappa \eta_{\text{conv}}} \right)^{\beta} k \Delta T^{1+\beta} \Delta z_{\text{conv}}^{3\beta-1}, \quad (15)$$

where the thermal diffusivity $\kappa = 1.47 \times 10^{-6} \text{ m}^2 \text{ s}^{-1}$ and the thermal expansion coefficient $\alpha = 1.56 \times 10^{-4} \text{ K}^{-1}$ stand for ice I, and η_{conv} is the viscosity of the convective layer of thickness Δz_{conv} . The viscosity η depends on temperature as

$$\eta(T) = \eta_0 \exp \left[27 \left(\frac{T_m}{T} - 1 \right) \right], \quad (16)$$

with $\eta_0 = 5 \times 10^{13} \text{ Pa s}$, the viscosity at the melting temperature T_m . The temperature difference ΔT across the convective layer is twice the temperature difference across the two thermal boundary layers (ΔT_{TBL}) given by (Sotin & Tobie 2004)

$$\Delta T_{\text{TBL}} = T_m - T_{\text{conv}} = -1.43 \times \left[\frac{\partial \ln(\eta)}{\partial T} \Big|_{T=T_{\text{conv}}} \right]^{-1}, \quad (17)$$

where T_m and T_{conv} are the melting temperature and the temperature in the convective well-mixed adiabatic ice layer.

Spohn & Schubert (2003) use typical values $b = 0.2$ and $\beta = 0.25$, while Deschamps & Sotin (2001) use $b = 0.79$ and $\beta = 0.263$. Large b -values correspond to very efficient heat transport by convection. Then, the temperature remains close to the surface temperature, and hardly reaches the melting temperature. The presence of ice is favored. On the contrary, low b -values favors the presence of an ocean below a convective ice layer. In the following, we will consider both sets of values for b and β .

4.3. Constraints on the Presence of Liquid Water

4.3.1. Method

To have a liquid layer below the ice shell, the temperature must reach the melting temperature above the triple point I/III/liquid at 0.21 GPa and 251 K; in other words, the temperature gradient below the surface must be steep enough to reach the melting temperature within the ice-I shell. Then, below this level, we have an ocean whose depth is limited by the pressure above which the liquid water is compressed into high-pressure ice (Fig. 4 and 5).

Using the equations of § 4.1 and 4.2, we can evaluate the minimum pressure – when only conduction drives the heat flow – and the maximum pressure – when there is a convective layer below a conductive lid – at which the temperature reaches the melting temperature. If the minimum pressure is larger than the triple point pressure, no ocean is possible below the ice shell. If the maximum pressure is smaller than the triple point pressure (i.e., if the temperature reaches the melting temperature despite the very efficient heat transfer by a convective layer), then the presence of an ocean is warranted.

4.3.2. Results

Taking the temperature profile obtained when only conduction drives the heat flow (Fig. 6), we see that it does not reach the melting temperature in the 0.025 and 50%wt cases. Therefore, an ocean within the ice-I shell of OGLE-2005-BLG-390Lb cannot be present. In the 0.025%wt case, there is simply not enough water and the maximum temperature reached at the bottom of the ice shell is in any cases well below 150 K. Thus, no liquid water is possible. In the 50%wt case, deeper in the planet, the maximum temperature reached at the bottom of the ice-II shell is in any cases well below 250 K. This does not allow for the presence of liquid water either.

Only in the 25%wt case, the temperature profile crosses the melting curve, although it does so below the triple point I/III/liquid, at pressure of about 0.5 GPa. This means that conduction alone is not able to transfer the heat from below across the solid ice shell. A conductive equilibrium does not exist in this case and the temperature profile plotted in Fig. 6 is not realistic.

Convection is likely to set up in the high-pressure ice and the temperature gradient can be steeper than the one calculated with conduction only. Using eq. (15) for the heat flow at 10 Gyr and other equations of § 4.2, and taking the parameters b and β typical

of a very efficient heat transport by convection (Deschamps & Sotin 2001), we find that the convective layer can be thick enough to allow the heat to be transferred without the temperature reaching the melting temperature. The presence of liquid water is not allowed in that case. However, if less efficient convection is considered by using smaller b -values (Spohn & Schubert 2003), we find that the temperature can effectively reach the melting temperature within the ice-II layer. In this very last case, solid-state convection cannot evacuate the heat from below, therefore the ice-II/v shell must be partly melted.

Nevertheless, in all the cases considered, the temperature profile never crosses the melting curve above $p_I = 0.21$ GPa. Therefore, an ocean cannot exist between ice I and higher-pressure ices.

4.3.3. Conclusion

Our study in which (i) the surface temperature is as cold as the equilibrium temperature, (ii) the ice is pure H₂O-ice, and (iii) the internal heat only consists in the radiogenic heat, implies that the ice-I shell of OGLE-2005-BLG-390Lb must be entirely frozen whatever the amount of water and the mass of the planet. Thus, no ocean can be present between ice I and high-pressure ice.

Only in the case of an intermediate amount of water, around 25%wt, there is a possibility to have liquid water within the ice-II/v shell because both thermal conduction and low-efficient solid-state convection are unable to remove the internal heat of the planet. If, however, solid-state convection is as efficient as proposed by Deschamps & Sotin (2001), then no liquid water exist in the ice-II/v layer of the 25%wt case.

In fact, the existence of liquid water is the result of a competition between two fundamental parameters: the heating h'_{rad} on one hand and the thickness of the ice layer on the other hand. Given the mass of the planet, the more water the planet contains, the less massive the silicate mantle is, and thus the more water in the planet, the less radiogenic heat there is to warm the ice. Meanwhile, the more water in the planet, the thicker the ice shell can be. Therefore, higher temperatures can be reached in the ice shell above the silicate mantle. This competition explains why the intermediate case with 25%wt water appears to be the most favorable for the presence of liquid water in OGLE-2005-BLG-390Lb, while in both 0.025 and 50%wt cases, there are no possibilities for the presence of liquid water.

5. VARYING PARAMETERS

In the previous section, we found that if the surface temperature of OGLE-2005-BLG-390Lb is equal to the equilibrium temperature (from 35 to 47 K for planetary masses of 3 to 11 M_{\oplus} , respectively) and the ice composition is 100% H_2O , then no oceans can be found between ice-I and high-pressure ices. We will discuss now the effects of a surface temperature larger than the equilibrium temperature, of a different composition of the ice, and finally of a larger internal heating.

5.1. Effect of an Increase in Surface Temperature

The possibility of the presence of an atmosphere thick enough to trigger a greenhouse effect or a smaller albedo could rise significantly the surface temperature. For instance, an albedo close to zero would increase the equilibrium temperature by a factor $\sqrt[4]{2}$, that is about 19%. Therefore, we shall evaluate the minimum increase in the surface temperature that allows the existence of an ocean between low- and high-pressure ices.

As a first approach, we can calculate the maximum temperature at the pressure p_I of the triple point I/III/liquid with thermal conduction only (§ 4.1). On one hand, for a given heat flow and at the pressure of the triple point corresponding to the base of the low-pressure ice shell, there is a diffusive coefficient $\delta(p_I)$. On the other hand, the ratio of the melting temperature at the triple point ($T_{mI} = 251$ K) to the actual surface temperature (T_{surf}) is equivalent to a minimum diffusive coefficient above which the water can melt. An ocean could exist if the increase of the surface temperature is above ΔT_{surf} where

$$\delta(p_I) \times (T_{surf} + \Delta T_{surf}) = T_{mI}. \quad (18)$$

Using this equation, we find that an increase of the surface temperature of at least [40,55], [65,80], and [100,115] K, for the 0.025, 25, and 50%wt cases, respectively, are required in order to partly melt the ice layer. However, those values cannot be obtained with smaller albedo and are unlikely to result from a greenhouse effect, given the small energy the planet is receiving from its star and the tenuous atmosphere of N_2 .

5.2. Effect of Ice Composition

We have assumed that the ice shell of OGLE-2005-BLG-390Lb is only made of the different phases of H_2O . However, due to the low temperature at the surface of the planet

(from 35 to 47 K, see § 2.2), not only H₂O, but also NH₃, CH₄, and possibly N₂ can condense. An accurate model of the ice shell would therefore need including these species in addition to H₂O, but is beyond the scope of this paper. A number of detailed studies have shown that a mixture of H₂O and, e.g., NH₃ crystallizes at a lower temperature than pure H₂O (see, e.g., Sotin et al. 1998; Spohn & Schubert 2003). The melting curve of this mixture is plotted in Figs. 3 and 6.

It shows that our previous results remain unchanged. In fact, the maximum temperatures calculated at the base of the ice-I shell are below the crystallizing temperature of both ammoniated and pure water in all cases. Therefore, no ocean is possible below the ice-I lid, even with the presence of NH₃.

5.3. Effect of an Increase in the Internal Heating

Similarly to the estimation of the surface temperature in § 5.1, we can calculate how much the internal heating has to be increased in order to partially melt the frozen ice shells. The minimum heat production h'_{liq} above which the temperature can reach the melting temperature $T_{m\text{I}}$ at pressure of the triple point I/III/liquid, p_{I} , can be estimated using results of § 4.1 and is given by:

$$h'_{\text{liq}} = h'_{\text{rad}} \times \frac{\ln [T_{m\text{I}}/T_{\text{surf}}(M_P)]}{\ln [\delta(p_{\text{I}}, h'_{\text{rad}})]}. \quad (19)$$

We find that the heat production calculated at 10 Gyr has to be multiplied by a factor of at least 1.6 to 1.9 in order to have liquid water in the 0%wt H₂O case, a factor of 2.1 to 2.5 in the 25%wt H₂O case, and 3.2 to 3.8 in the 50%wt H₂O case.

If we allow for convection as in § 4.2, we obtain larger heat production rate. If we use small values of b corresponding to a convection inefficient for the transport of the internal heat, the results are barely changed. If we assume a much more efficient convection in the ice-I shell, we find that the heating rates needed to obtain liquid water are 75 to 100% larger than those obtained by neglecting the convection. For instance, for a 5.5-M_⊕ planet with 25%wt H₂O, the heating rate needed to reach the melting temperature within the low-pressure ice is 3.9 and 2.2 higher than the heating at 10 Gyr, for a large and a small b , respectively. Those results are barely changed by the possible presence of NH₃.

Although the present-day OGLE-2005-BLG-390Lb is likely to be entirely frozen, the heating needed to have liquid water below the surface of this planet is only a factor-of-a-few larger than the calculated radiogenic heating at 10 Gyr. It must be recalled that this radiogenic heating is only a minimum: a remnant heat from the accretion is certainly not

negligible, in particular for such a massive planet. A comparison with the Earth shows that it could be of the same order as the radiogenic heating. Moreover, in the past the radiogenic heat was larger. Using eq. (6), the radiogenic heat is a factor of 2 and 4 larger when the planet was 4.4- and 1.8-Gyr old. This allows us to suggest that liquid water was certainly present in the past during several billion years below the surface of OGLE-2005-BLG-390Lb.

6. CONCLUSIONS

Because OGLE-2005-BLG-390Lb orbits a few AU away from a faint M star and is about 10-Gyr old, this planet is likely to be entirely frozen.

In the favored scenario, the planet has no heavy atmosphere and its surface temperature is close to the equilibrium temperature of a black body (35 to 47 K); then, the surface should be entirely frozen.

If the planet contains terrestrial amounts of water (or much more), a $\lesssim 10$ -km- (or $\gtrsim 1000$ -km-) thick ice mantle can be present. The radiogenic heat production rate, which depends on the quantity of water/silicates contained in the planet, is probably not sufficient to prevent a potential sub-surface ocean from freezing completely at the likely age of 10 Gyr.

However, remnant heat and larger radiogenic heating in the past allow us to suggest that a liquid ocean must have been present during several billion years. In similarity with the icy satellites of the Solar system, this liquid water was located below low-pressure ice I. At the bottom of the ocean, either a silicate mantle or high-pressure ices could be found, for water-poor or water-rich planet, respectively.

In some respects, OGLE-2005-BLG-390Lb opens a new frontier in modeling extra-solar planets: not only because it is presently the closest planet to the Earth in terms of mass, but also because it is located at the cold border of its planetary system, beyond the snowline. Up to now, the greatest interest has been shown in observing and modeling hot Jupiters and planets close to their star, mainly because they were the first to be detected. Microlensing detection technique has now the potential to unveil a population of ice giants, frozen ocean-planets, and other snowball Earths. The present work is a first approach to such objects. It opens new perspectives for exoplanetology.

We warmly thank Christophe Sotin and Alain Léger for useful advices and comments about the manuscript, Roger Ferlet for thorough reading and wise suggestions, and the referee Hauke Hussmann for a constructive review.

REFERENCES

- Baraffe, I., Chabrier, G., Allard, F., & Hauschildt, P. H. 1998, *A&A*, 337, 403
- Beaulieu, J.-P., Bennett, D. P., Fouqué, P., et al. 2006, *Nature*, 439, 437
- Bercovici, D., Schubert, G., & Reynolds, R. T. 1986, *Geophys. Res. Lett.*, 13, 448
- Cox, A. N. 2000, *Allen’s Astrophysical Quantities*, ed. A. N. Cox, Springer (4th ed.; Springer)
- Deschamps, F., & Sotin, C. 2001, *J. Geophys. Res.*, 106, E3, 5107
- Dominik, M. 2006, *MNRAS*, 367, 669
- Fei, Y., Mao, H.-K., & Hemley, R. J. 1993, *J. Chem. Phys.*, 99, 7, 5369
- Hemley, R. J., Stixrude, L., Fei, Y., & Mao, H.-K. 1992, in *High Pressure Research: Applications to Earth and Planetary Sciences*, ed. Syono Y. & M. H. Manghnani (AGU Monogr.), 183
- Hussmann, H., Spohn, T., & Wiczerkowski, K. 2002, *Icarus*, 156, 143
- Kasting, J. F., Whitmire, D. P., & Reynolds, R. T. 1993, *Icarus*, 101, 108
- Klinger, J. 1980, *Science*, 209, 271
- Lecavelier des Etangs, A. 2006, *A&A*, submitted
- Léger, A., Selsis, F., Sotin, C., et al. 2004, *Icarus*, 169, 499
- Lide, D. R. 2005, *Handbook of Chemistry and Physics* (85th ed.; CRC Press)
- Lovis, C., Mayor, M., Pepe, F., et al. 2006, *Nature*, 441, 305
- Rivera, E. J., Lissauer, J. J., Butler, R. P., et al. 2005, *ApJ*, 634, 625
- Santos, N. C., Bouchy, F., Mayor, M., et al. 2004, *A&A*, 426, 19
- Sicardy, B., Widemann, T., Lellouch, E., et al. 2003, *Nature*, 424, 168
- Sotin, C., & Tobie, G. 2004, *C. R. Physique*, 5, 769
- Sotin, C., Grasset, O., & Beauchesne, S. 1998, in *Solar System Ices*, ed. B. Schmitt et al. (Kluwer Academic Publishers), 79
- Sotin, C., Grasset, O., & Mocquet, A. 2006, *Icarus*, submitted

Spohn, T., & Schubert, G. 2003, *Icarus*, 161, 456

Turcotte, D. L., & Schubert, G. 2002, *Geodynamics* (2nd ed.; Cambridge University Press)

Uchida, T., Wang, Y., Rivers, M. L., & Sutton, S. R. 2001, *J. Geophys. Res.*, 106, 21799

Vacher, P., Mocquet, A., & Sotin, C. 1998, *Phys. Earth Planet. Int.*, 106, 275

Valencia, D., O’Connell, R. J., & Sasselov, D. 2006, *Icarus*, 181, 545

Zoccali, M., Renzini, A., Ortolani, S., et al. 2003, *A&A*, 399, 931

Table 1. Parameters of the microlensing event OGLE-2005-BLG-390.^a

Parameter	Symbol	Value
planet-to-star mass ratio	q	$(7.6 \pm 0.7) \times 10^{-5}$
projected separation	d	$1.609 \pm 0.004 R_E$
distance to the source	D_S	8.5 kpc
distance to the lens	D_L	7.2 ± 0.8 kpc
mass of the star ^b	M_\star	$0.22^{+0.21}_{-0.11} M_\odot$
mass of the planet ^b	M_P	$5.5^{+5.5}_{-2.7} M_\oplus$
semi-major axis ^b	a	$2.6^{+1.5}_{-0.6}$ AU

^aFrom Beaulieu et al. (2006).

^bThe quantity is the mean value of the probability distribution.

Table 2. Properties of long-lived radioactive isotopes in the Earth’s interior.

Isotope	Heat Production h (W kg ⁻¹)	Half-Life $\tau_{1/2}$ (Gyr)	Concentration X (kg kg ⁻¹)
²³⁸ U	9.37×10^{-5}	4.47	25.5×10^{-9}
²³⁵ U	5.69×10^{-4}	0.704	1.85×10^{-10}
²³² Th	2.69×10^{-5}	14.0	1.03×10^{-7}
⁴⁰ K	2.79×10^{-5}	1.25	3.29×10^{-8}

Note. — The concentration given are the value in the Earth mantle. From Cox (2000), referring to Turcotte & Schubert (1982).

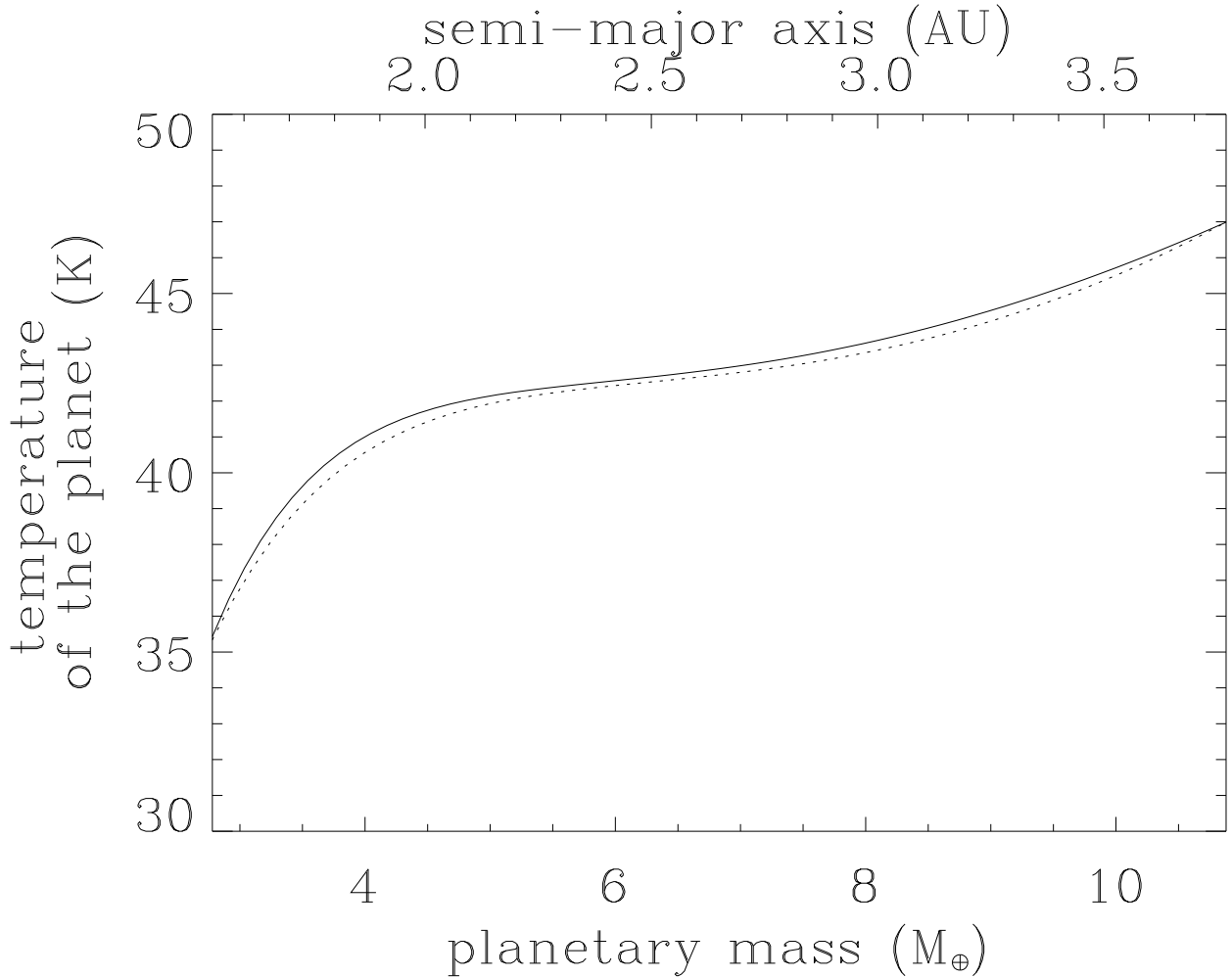


Fig. 1.— Possible surface temperatures of the planet. In our case, the properties of the star are depending on the mass of the planet ($M_{\star} = M_P/q$ where $q = 7.6 \times 10^{-5}$, and $L_{\star} \equiv L_{\star}(M_{\star})$, as expressed in eq. [1] and eq. [3], respectively). In addition, the semi-major axis depends on M_{\star} (eq. [2]) and thus on M_P . The surface temperature is calculated assuming it is equal to the equilibrium temperature with an albedo of 50%, and is represented here as a function of the planetary mass ($T_{\text{surf}} \equiv T_{\text{surf}}(M_P)$, bottom axis, plain line) and semi-major axis ($T_{\text{surf}} \equiv T_{\text{surf}}(a[M_P])$, top axis, dotted line), accordingly to eq. (4). As a result, the temperature of the planet evolves counter-intuitively with the semi-major axis: the larger the separation between the planet and its star, the *higher* the surface temperature is. This is because the stellar luminosity is not constant, but rather becomes more intense as both the planetary and stellar masses increase (eq. [3]).

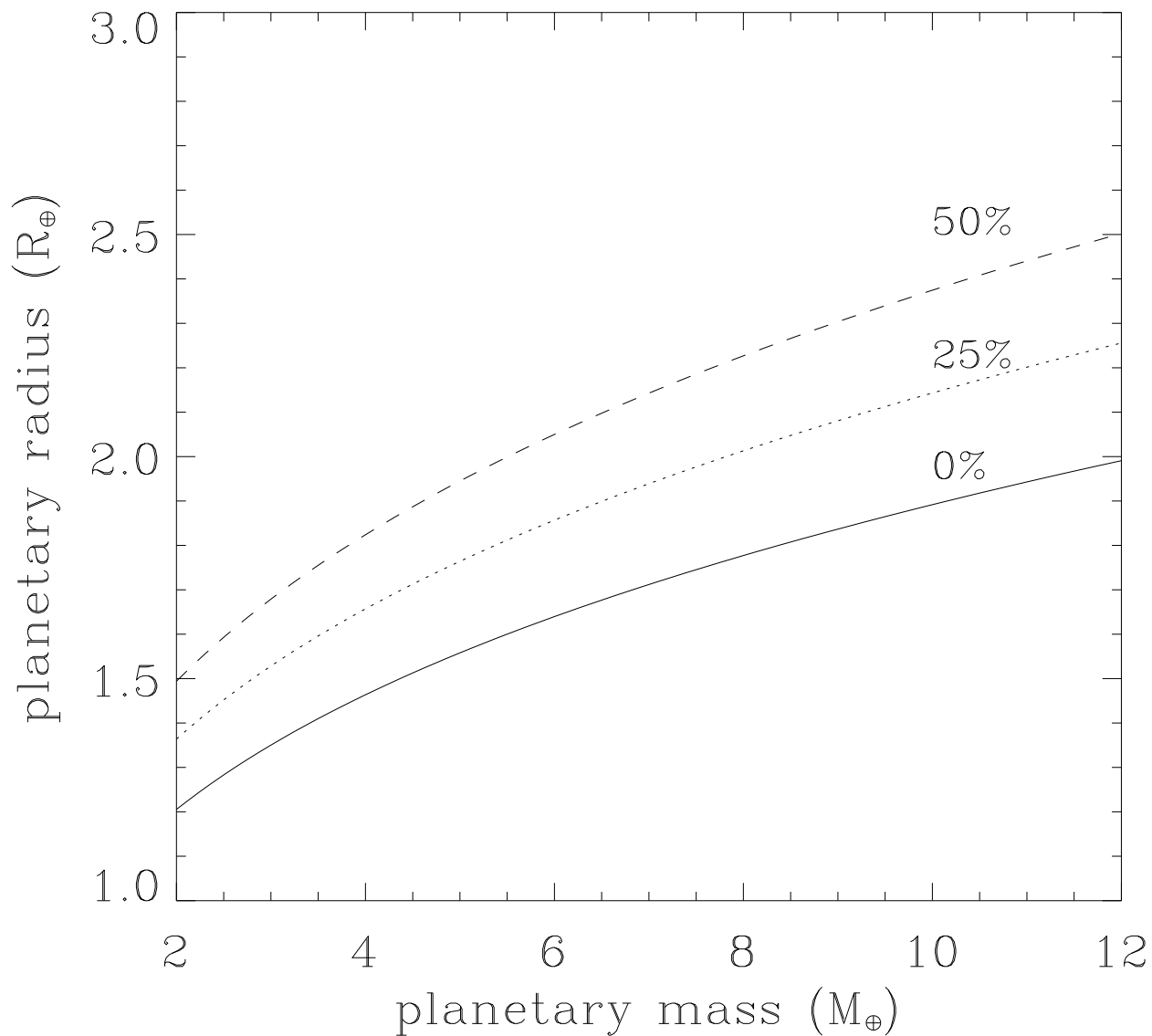


Fig. 2.— Radius of the planet as a function of the planetary mass. The radius is calculated using a mass-radius relation from Sotin et al. (2006), for different H₂O mass fractions: 0.025%wt (noted 0%wt, plain line), 25%wt (dotted line), and 50%wt (dashed line).

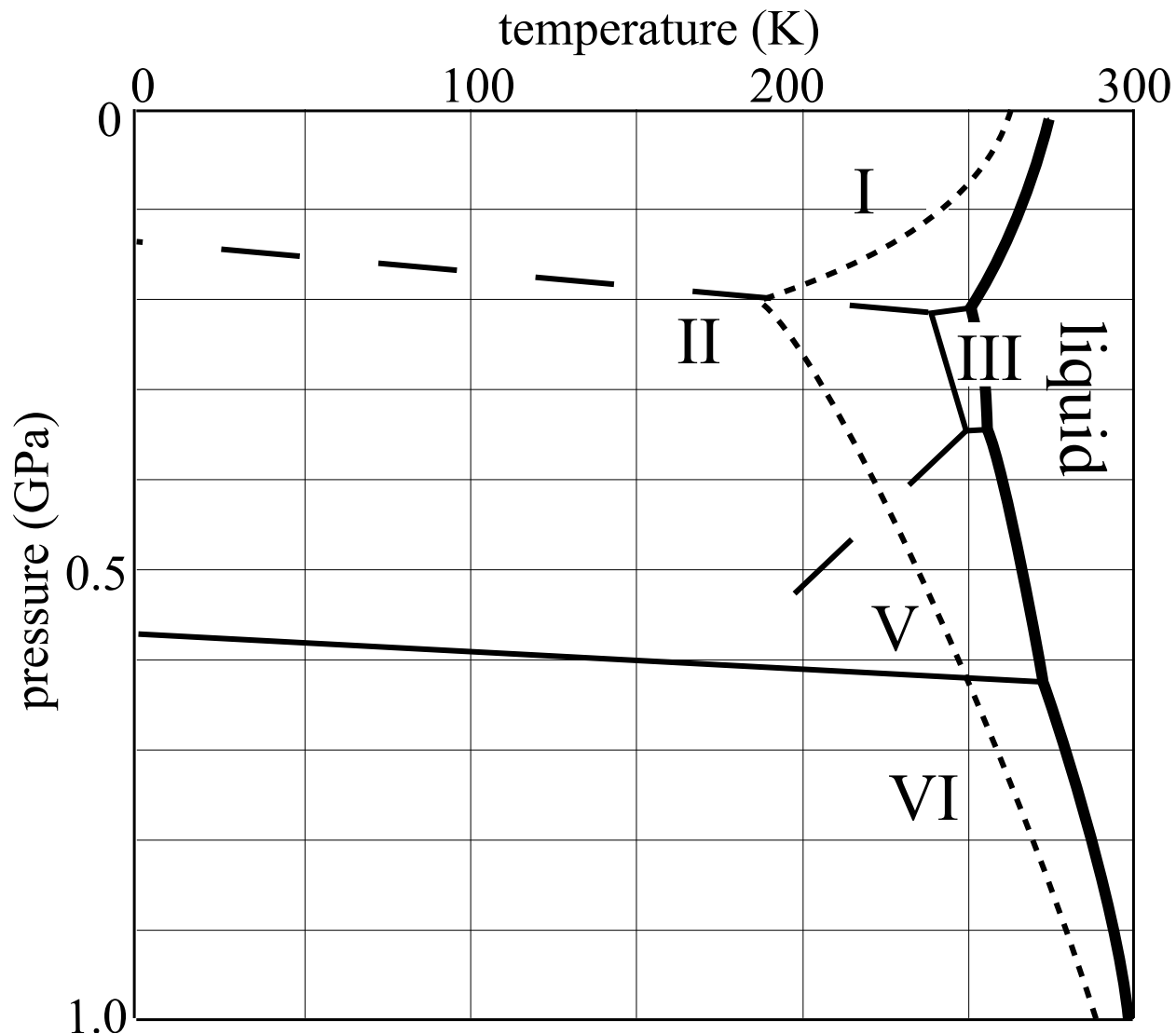


Fig. 3.— Phase diagram of water. The domains of existence in pressure and temperature of the liquid phase and five solid phases are figured. The thick line is the phase boundary between the different ices and liquid water, i.e., the melting curve. Each phase of ice corresponds to a given crystalline structure. Hexagonal ice I presents the particularity of being less dense than liquid water. Besides, its melting curve has a negative slope: ice I can melt under pressure if $T > 250$ K. On the contrary, the high-pressure phases represented here (ices II, III, V, and VI) are all denser than liquid water. As a consequence, a liquid layer of water can exist below an ice-I layer and above a ice-III, -V, or -VI layer. This is the favored structure for the ice shells of the icy moons in the Solar System, although such ice shells are usually modeled assuming ammoniated (with NH_3) rather than pure liquid H_2O . Such a mixture crystallizes at lower temperature than pure H_2O (dashed line).

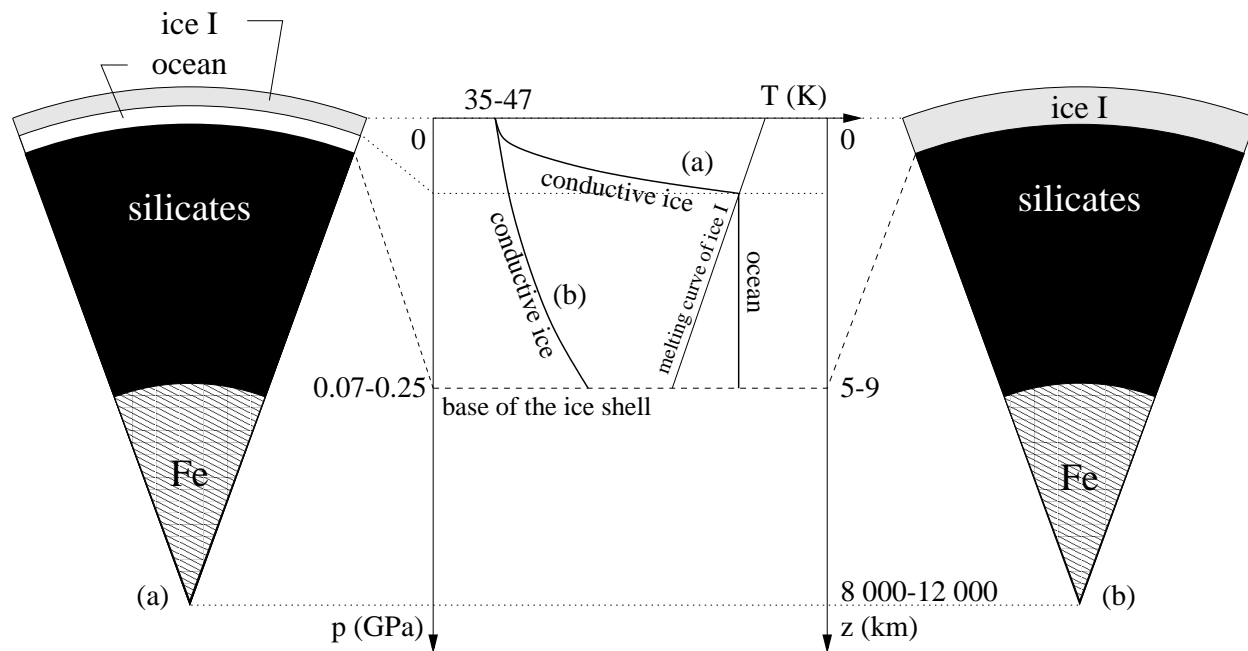


Fig. 4.— Possible internal structures for a water-poor OGLE-2005-BLG-390Lb, with typically a terrestrial fraction of water (0.025%wt). In this case, the planet is composed by a metallic core (hatching) and a silicate mantle (black). The water can be present in the form of a thin (5–9 km) layer of low-pressure ice I (grey). Two possible pressure-temperature profiles across the ice shell are sketched at the center (thick lines), assuming the ice is conducting the heat from the base of the shell up to the surface. If the temperature at the base of the ice shell is lower than the melting temperature of ice I (thin line) then the layer is completely frozen (b). However, if the temperature at the base is above the melting temperature then an ocean (white) can exist below the ice (a). Note that in any cases, the H₂O layer would remain rather thin compared to the radius of the planet. *The figure is not to scale.*

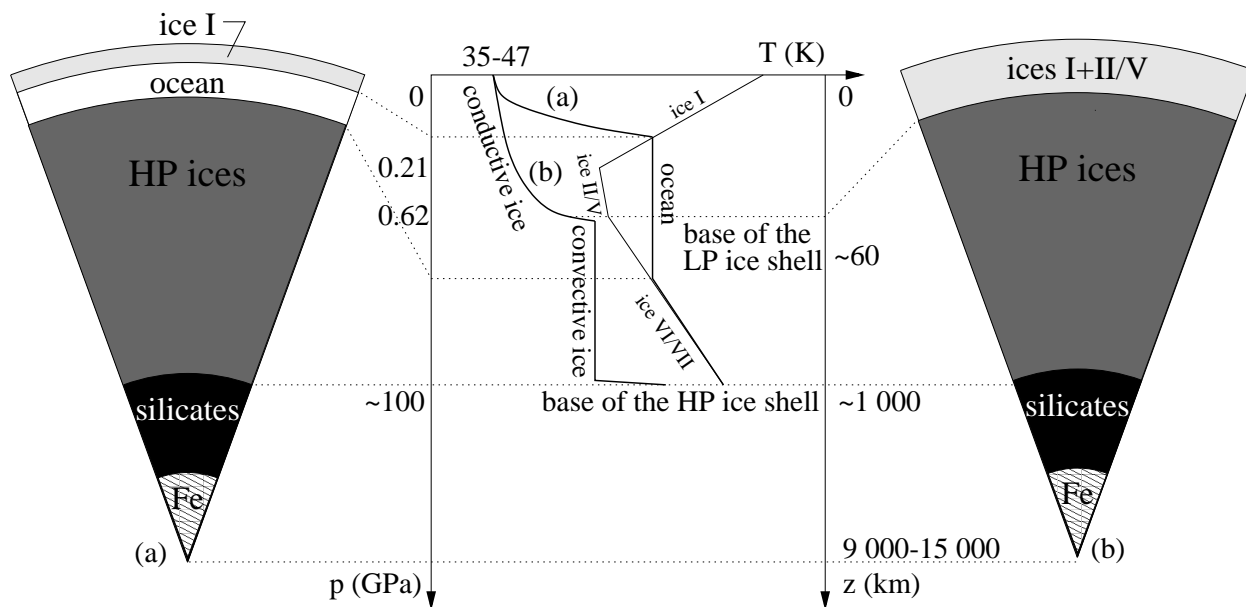


Fig. 5.— Possible structure for a water-rich OGLE-2005-BLG-390Lb. The mantle (black)-to-core (hatching) mass ratio is still fixed to $\sim 2/1$, as for the water-poor cases in Fig. 4, but here a large part of the planetary mass is accounted for by a high-pressure ice mantle (dark grey). It is overtopped by a low-pressure ice shell consisting in ice I and, depending on the temperature, liquid water, ice II, or ice V. The base of the low-pressure ice shell is the phase boundary between ices II/V and VI at 0.62 GPa (see Fig. 3). The temperature-pressure profile across the low-pressure ice shell (light grey) is plotted at the center in two cases (thick lines), both assuming the heat is transferred by conduction across the low-pressure ice shell. In case (a), the profile crosses the melting curve of ice I (thin line) and an ocean (white) exists between the low- and high-pressure ice shells. The temperature profile then follows the melting curve from the base of the low-pressure ice shell down to the base of the high-pressure ice shell. In case (b), the temperature profile does not cross the melting curve of ice I, so that the low-pressure ice shell is entirely frozen. At the base of the low-pressure ice shell, the conductive profile becomes convective. *The figure is not to scale.*

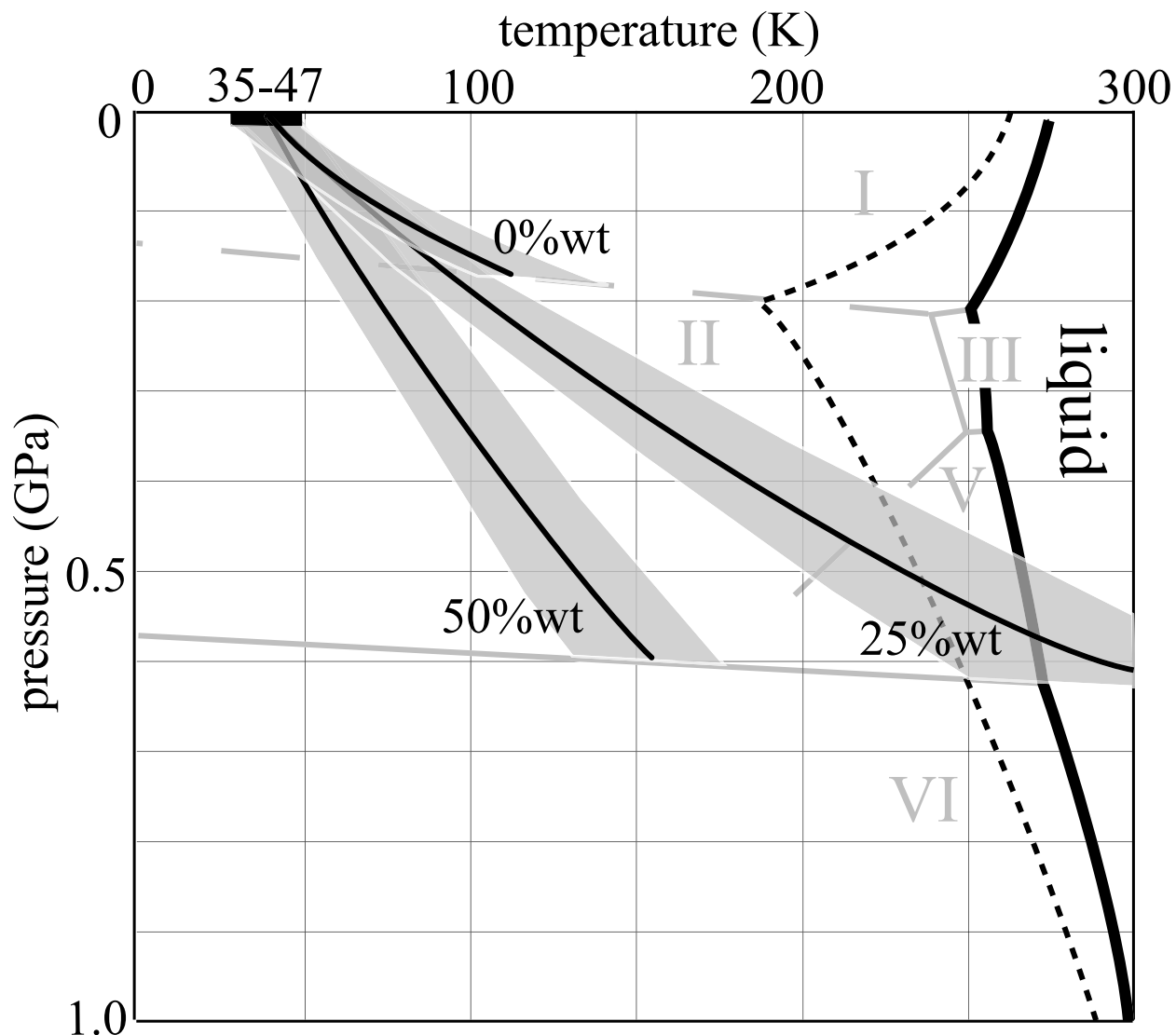


Fig. 6.— Temperature profiles obtained with the diffusive model in which the heat flow is transferred only through thermal conduction. The profiles are calculated across the low-pressure ice shell in the 0.025%wt (i.e., the ice-I layer), 25, and 50%wt (ice-I/II layer) cases. For each case, the profile is depending on the planetary mass. The surface temperature is correlated to the planetary mass so that the surface temperature varies from 35 to 47 K (thick horizontal black line) when the mass varies from 3 to 11 M_{\oplus} . The possible profiles are represented (grey area) for each case. The temperature profile for the most probable mass ($5.5 M_{\oplus}$) is evidenced (black line). Thermal conduction is sufficient to evacuate the heat from below in the 0 and 50%wt cases, either the ice is pure or NH_3 -mixed H_2O . Indeed, the temperature profiles do not cross the melting curves (thick and dashed lines, respectively) for both ice compositions. In the 25%wt case, the temperature profile crosses the melting curve. However this is a maximum temperature curve. Convection is likely to set up and, by efficiently transferring the heat, to avoid the temperature to reach the melting temperature (see text).